Journal of Molecular Structure 1312 (2024) 138521

Contents lists available at ScienceDirect

Journal of Molecular Structure

journal homepage: www.elsevier.com/locate/molstr

# Colour tuning in $Sm^{3+}$ activated and $Sm^{3+}/Eu^{3+}$ co-activated $SrBi_4Ti_4O_{15}$ phosphors for w-LED applications

Pooja Rohilla [a], Sheetal Kumari [a], Ravita [b], Samarthya Diwakar [c], Rupesh Talewar [d], Ankur Shandilya [e], Kartika Maheshwari [f], M. Venkateswarlu [g], Aman Prasad [c,*], A.S. Rao [a]

[a] Department of Applied Physics, Delhi Technological University, Delhi 110042, India
[b] Department of Physics, Chaudhary Bansi Lal University, Bhiwani 127021, India
[c] Department of Physics and Computer Science, Dayalbagh Educational Institute (DEI), Deemed University, Agra 282005, India
[d] Department of Physics, Shri Ramdeobaba College of Engineering and Management, Katol Road, Nagpur 440013, India
[e] Department of Physics, Hindu College, University of Delhi, Delhi 110007, India
[f] ABES Engineering College, Ghaziabad 201009, India
[g] Department of Physics, Koneru Lakshmaiah Education Foundation, Vaddeswaram, Guntur 522502, India

ARTICLE INFO

*Keywords:*
BLSP structure
Decay Kinetics
w-LEDs
TDPL
Kubelka-Munk theory

ABSTRACT

$SrBi_4Ti_4O_{15}$ (SBT) phosphors activated by $Sm^{3+}$ and co-activated by $Eu^{3+}$ have been synthesized in the current research using a straightforward solid-state reaction technique. X-ray Diffraction (XRD) confirms the sample's crystallinity. Scanning electron microscopy (SEM), energy dispersive x-ray spectroscopy (EDX), and elemental mapping have been used to analyse the morphology and elemental composition of the synthesized phosphor. Fourier-transform infrared spectroscopy (FT-IR) analysis has confirmed the vibrational characteristics of the as prepared phosphor. Photoluminescence studies show increase in luminescence intensity in case of $Sm^{3+}/Eu^{3+}$ co-activated phosphors as compared with singly doped $Eu^{3+}$ and $Sm^{3+}$ activated SBTO phosphors. Colour tunability was also observed from reddish-orange to pure red region when $Sm^{3+}$ activated phosphors were co-activated with $Eu^{3+}$ ions. These outcomes demonstrate that $SrBi_4Ti_4O_{15}$ phosphors activated or co-activated with $Sm^{3+}$ and $Eu^{3+}$ can be deployed in w-LEDs and other display devices applications.

## 1. Introduction

There is an increasing need for high-quality white light with certain colour temperatures and colour rendering qualities as lighting technology develops [1,2] . Researchers are striving to create phosphors that can accurately and faithfully produce a variety of hues. In numerous optoelectronic devices, such as lasers, LEDs, and photovoltaics, phosphors are crucial [3]. Energy sustainability as a whole is improved by the energy savings brought about by better phosphor materials. Researchers today strive to improve how well can phosphor materials transform light. This entails enhancing phosphors' quantum efficiency, reducing energy losses during the conversion process, and enhancing the spectral dispersion of produced light, among other things. When ultraviolet (UV) and visible light are utilised alternately, photochromism occurs, which is a reversible colour change. Due to their many uses, including photo switches, sensors, 3D homographic memories, and smart windows, photochromic materials have attracted a lot of attention. For this reason, scientists are looking at new phosphor materials that could enhance the functionality of these devices and open up new possibilities. In contemporary lighting technology, phosphor-based LEDs, sometimes referred to as phosphor-converted LEDs (pc-LEDs), are essential. By employing a blue or UV LED chip to activate a phosphor substance, these LEDs are made to create white light. The phosphor emits light in the visible spectrum, usually at blue and yellow wavelengths that combine to produce white light. Nowadays, w-LEDs are created by coating the GaN blue LED chip with YAG: $Ce^{3+}$ yellow phosphors [4]. In any case, the lack of red emission causes these w-LEDs to exhibit certain drawbacks including high correlated colour temperature (CCT) and low color-rendering index (CRI), which restrict their adaptability in a variety of applications [5]. We can create an acceptable colour temperature and CRI for residential, commercial, and architectural lighting by combining blue or UV LEDs with red-emitting phosphors. For lighting and display technology to provide a wide spectrum of colours, red-emitting phosphors are essential [6].

* Corresponding author.
*E-mail address:* amanprasad2891@gmail.com (A. Prasad).

https://doi.org/10.1016/j.molstruc.2024.138521
Received 7 December 2023; Received in revised form 24 April 2024; Accepted 30 April 2024
Available online 1 May 2024

To suit the changing needs of many industries, researchers are attempting to create new and superior red-emitting phosphor materials with improved efficiency, stability, and colour purity. Red-emitting phosphors are used by the entertainment and consumer electronics industries to create precise and vibrant colours in colour TVs, monitors, and projectors. Research into more efficient phosphor-based LEDs is motivated by the demand for energy-efficient lighting and decreased energy consumption. Numerous uses in lighting, displays, optoelectronics, and other fields are fuelling the demand for red-emitting phosphors [7,8].

The synthesis and photoluminescence (PL) behaviour of $SrBi_4Ti_4O_{15}$ (SBT) phosphors co-doped with $Sm^{3+}/Eu^{3+}$ ions have been described in this current work. SBT lattices are bismuth layered structure ferroelectrics (BLSFs) with predictable $(Bi_2O_2)^{2+}$ layer intergrowth. Due to its unique structure, low phonon energy, high chemical stability, low cost, non-toxic and environmental friendly behaviour, the Aurivillius phase (SBT) materials have attracted a lot of attention of researchers [9,10]. These bismuths layered structures also possesses high Curie temperature, good dielectric, ferroelectric and piezoelectric properties, which made them highly beneficial in other applications like piezoelectric, pyroelectric and non-volatile random access memory etc. [11,12]. On the other hand, due to their potential utility in solid-state lasers, displays, and other technologies, rare earth (RE) ions have been extensively exploited as luminescence centres throughout the past few decades. Yujian Wu et al., published their work on $SrBi_4Ti_4O_{15}$: $Er^{3+}$ emitting phosphor for anti-counterfeiting application [13]. Yuying Zhang et al. have studied the photoluminescence, electrical properties and electron band structure of $(Ho, Yb)^{3+}$ co-doped $SrBi_4Ti_4O_{15}$multifunctional ceramics [11]. Tong Wei et al. have published articles on high performance temperature sensing and optical heating of $Tm^{3+}$ and $Yb^{3+}$ co-doped $SrBi_4Ti_4O_{15}$ up-conversion luminescence nanoparticles and optical multi-functionalities of $Er^{3+}$ and $Yb^{3+}$ sensitized strontium bismuth titanate nanoparticles [10,14]. As per our knowledge, no work has been reported on $Sm^{3+}/Eu^{3+}$ SBT phosphors for w-LED applications. In this work, we have used samarium ($Sm^{3+}$) and europium ($Eu^{3+}$) RE ions as sensitizers/ activators to study the prospect of tuning orange-red emission to deep red in the as prepared SBT lattice for usage as red emitting component in w-LEDs and other lighting applications.

## 2. Experimental and characterization section

In this study, a solid-state reaction procedure under high temperature was used to generate a series of SBT: $xSm^{3+}$ ($x = 0.5$, 1.0, 1.5, and 2.0 mol%) and SBT: $xSm^{3+}/yEu^{3+}$ ($x = 1.0$ mol%, $y = 1.0$, 2.0, 3.0, 4.0, and 5.0 mol%) doped phosphors under air atmosphere. First, the raw materials $SrCO_3$ (98 %) (Thermo Fisher), $TiO_2$ (98 %) (Thermo Fisher),

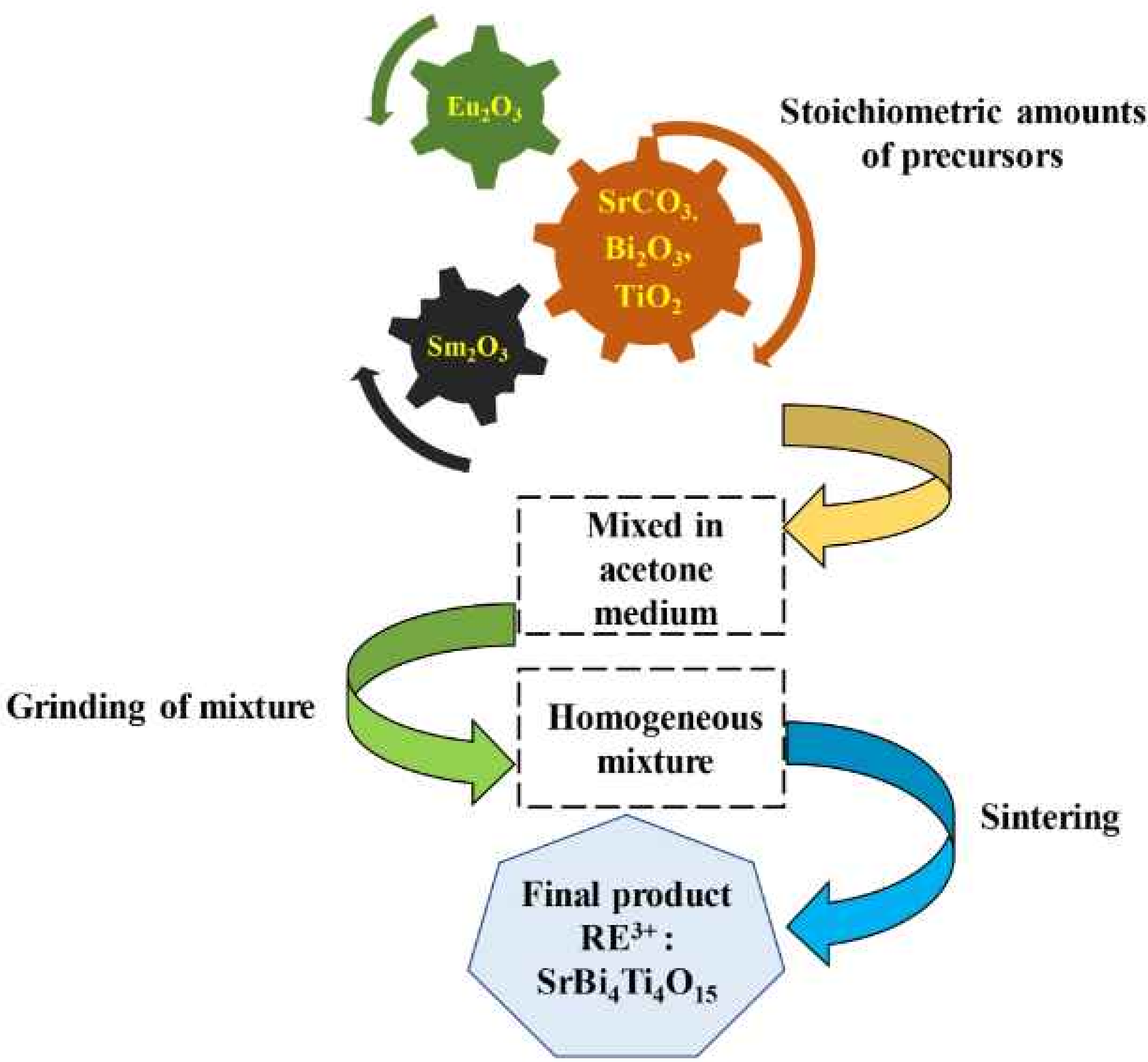


Fig. 1. Flow chart of various steps involved in the synthesis process of SBT phosphor.

$Bi_2O_3$ (99 %) (Loba Chemie), $Sm_2O_3$ (99 %) (Loba Chemie), and $Eu_2O_3$ (99 %) were weighed according to the stoichiometric proportion, placed in an agate mortar, and thoroughly ground for 60 min until a homogeneous mixture was obtained. The mix was then put into an alumina crucible and heated to a high temperature (900 °C) in a programmable furnace. Once the furnace naturally cooled to room temperature, the samples were ground again. Additional characterizations were performed using the obtained phosphor powder. Fig. 1 depicts all synthesis steps in detail.

The X-ray diffraction (XRD) patterns of the synthesised phosphors were captured using a Bruker D8 Advanced Powder X-ray diffractometer and a Cu-K radiation source (λ=1.54 Å, 40 kV, 40 mA) in the 2θ range of 20–80° Using a JEOL 7610F Plus microscope, the morphological, elemental, and EDX analyses of the materials were performed. The Perkin Elmer Spectrum 2 was used to examine the phosphor's vibrational modes and functional groups. At room temperature, diffuse reflectance spectra of synthesised samples were captured using a UV–Vis spectrophotometer (Jasco V-770 Spectrophotometer). Using a xenon lamp as the excitation source, the samples' excitation and emission spectra were recorded using a Jasco FP-8300 Spectrofluorometer. PL decay curves were recorded on a Hameg Instruments HM 1507 digital oscilloscope running at 150 MHz. Using an ocean optics system, the temperature-dependent photoluminescence (TDPL) emission spectra were measured. All PL measurements, except for TDPL, were recorded at room temperature.

## 3. Results and discussion

### 3.1. XRD analysis

The initial evaluation of the purity of the as-prepared sample involves phase confirmation using XRD. Fig. 2 displays the XRD patterns of the pure, undoped $SrBi_4Ti_4O_{15}$ base material. All the diffraction peaks observed in the sample match the standard data for $SrBi_4Ti_4O_{15}$ (ICDD no. 43–0973). There are no indications of the presence of any other phases, suggesting that the obtained samples are composed of a single phase. $SrBi_4Ti_4O_{15}$ possesses an orthorhombic crystal structure with a space group denoted as A21am (36). It has specific lattice parameters: $a = 5.4280$ Å, $b = 5.4380$ Å, $c = 40.9400$ Å, and angles α, β, and γ are all 90°

Fig. 3 depicts the structural configuration of $SrBi_4Ti_4O_{15}$, showcasing the positioning of $Sr^{2+}$, $Bi^{3+}$, and $Ti^{4+}$ atoms within their respective coordination environments. $SrBi_4Ti_4O_{15}$ is classified as an Aurivillius-type material, characterized by a pseudo-perovskite structure. This classification was first established by Aurivillius in 1949. Aurivillius-type oxides follow a general formula $[Bi_2O_2][A_{n-1}B_nO_{3n+1}]$ ($n = 1, 2, 3, 4$), where $[Bi_2O_2]^{2+}$ layers intertwine with perovskite-like $[A_{n-1}B_nO_{3n+1}]^{2-}$ layers [15]. $ABi_4Ti_4O_{15}$ ($A$ = Ba, Sr, and Pb) belong to the $n = 4$ series within the Aurivillius family. In the crystal structure of $SrBi_4Ti_4O_{15}$, titanium occupies the $MO_6$ position in the perovskite layer [16]. The coordination of atoms is as follows: Sr is coordinated with 8 oxygen atoms, Bi(1) and Bi(2) with 6 oxygen atoms, while Bi(3) is coordinated with 5 oxygen atoms. Hence, based on the ionic radii and valency of the doped rare earth ion, it is anticipated that rare earth ions will substitute Sr and Bi sites in the crystal structure. As we know, these

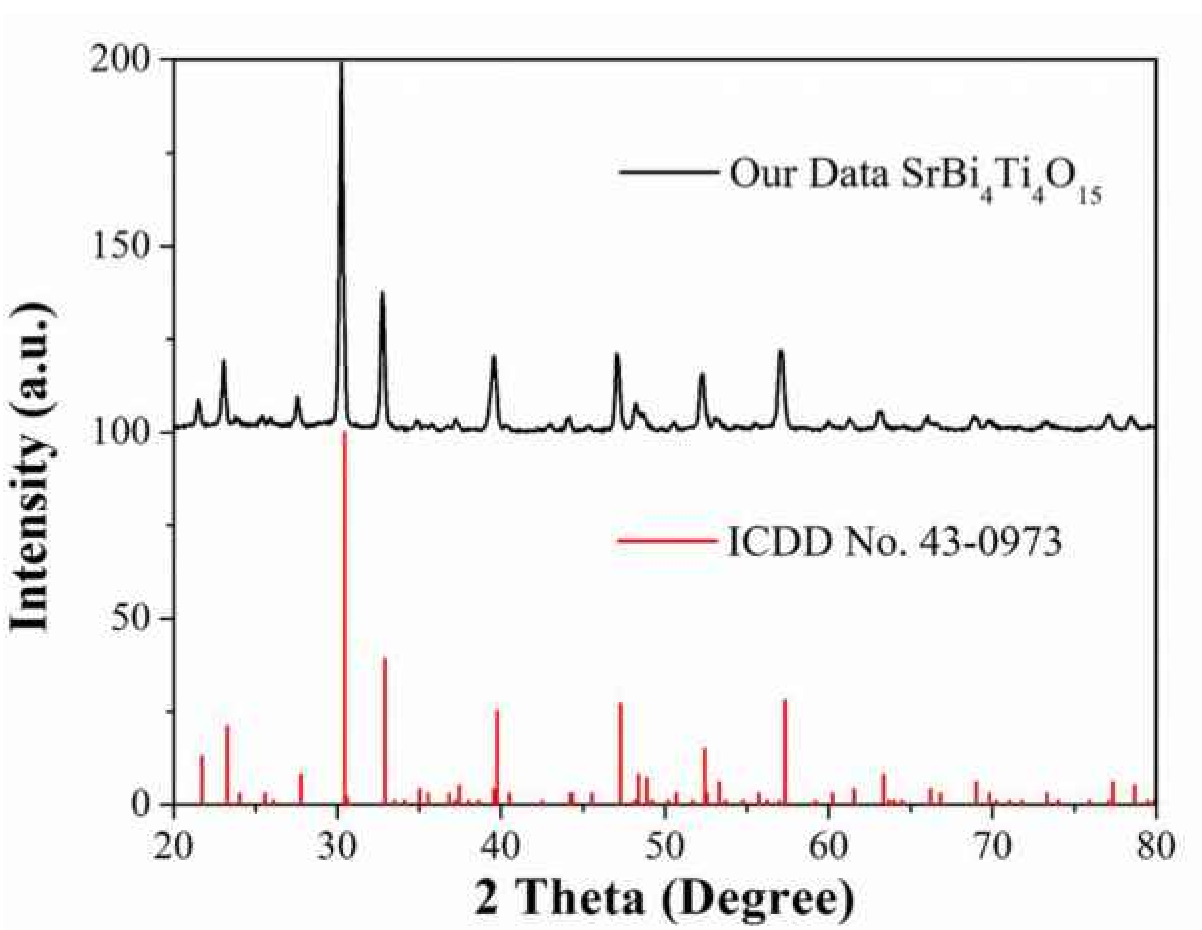


Fig. 2. XRD pattern of the $SrBi_4Ti_4O_{15}$ and the reference data of ICDD no. 43–0973.

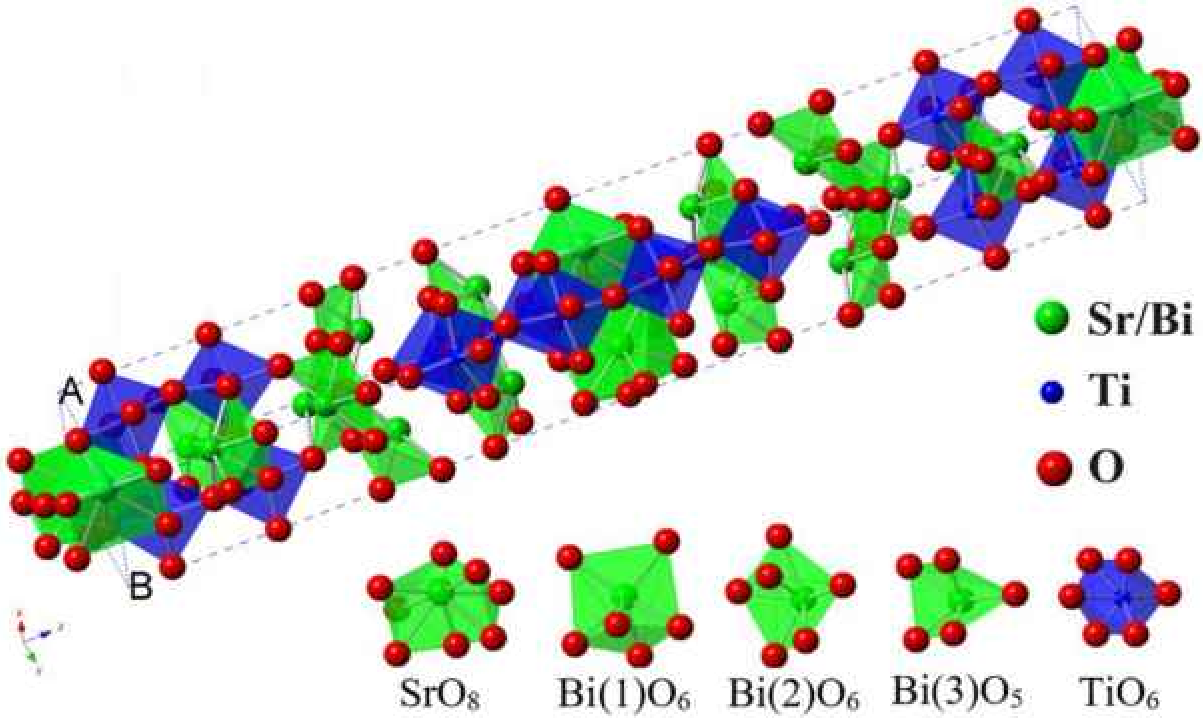


**Fig. 3.** Crystal structure of $SrBi_4Ti_4O_{15}$, emphasizing the coordination environment of Sr, Bi, Ti and O atoms.

lanthanides, exhibit unique electronic and magnetic properties that make them attractive for various technological applications. Substituting the RE ions in the crystal lattice of a phosphor can lead to changes in the emission wavelengths and color of the emitted light. This property is particularly important in applications like light-emitting diodes (LEDs) and display technologies.

### *3.2. SEM and EDX analysis*

$Sm^{3+}$ doped SBT phosphor and $Sm^{3+}/Eu^{3+}$ co-doped SBT phosphor's respective morphologies are shown in SEM micrographs presented in Fig 4(a & b). Small nanoparticles with variable orientation that resemble plates were observed [10]. It is thought that the intrinsic anisotropy of the bismuth layered perovskite structure is what that caused the plate-like grain development [14]. The range of prepared phosphors' particle sizes is 150–200 nm.

The EDX spectrum and elemental mapping of SBT:1mol% $Sm^{3+}$, 1mol% $Eu^{3+}$ phosphor have been displayed in Fig. 5 in order to examine its composition and element distribution [17]. According to the sample's EDX spectrum, $Eu^{3+}$, $Sm^{3+}$, $Sr^{2+}$, $Ti^{4+}$, and $Bi^{3+}$ elements make up the sample. These are the precursor substances that were used to create this phosphor. These elements are distributed equally according to the results of the elemental mapping, which further demonstrates the sample's accurate synthesis.

### *3.3. FT-IR analysis*

The FT-IR spectrum at room temperature has been shown in Fig. 6 in the range of 400–4000 $cm^{-1}$. At 557 and 853 $cm^{-1}$, two strong absorption peaks were seen wherein, the former peak could be attributed to Ti-O bond stretching and the latter was attributed to Bi-O bond stretching vibration [18]. The creation of a layered-perovskite structure

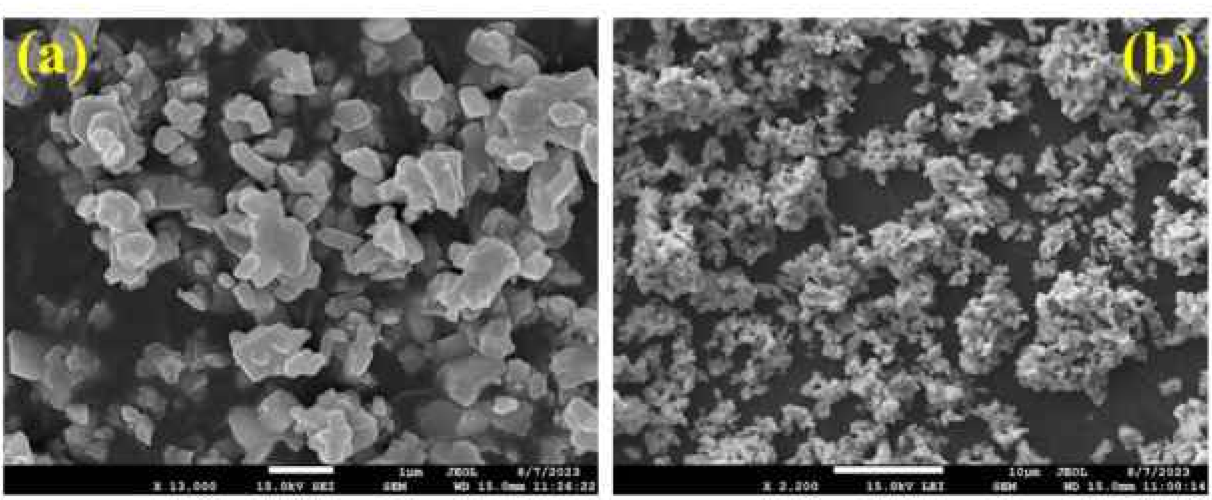


**Fig. 4.** SEM images of $Sm^{3+}$ doped SBT phosphor and $Sm^{3+}/Eu^{3+}$ co-doped SBT phosphors.

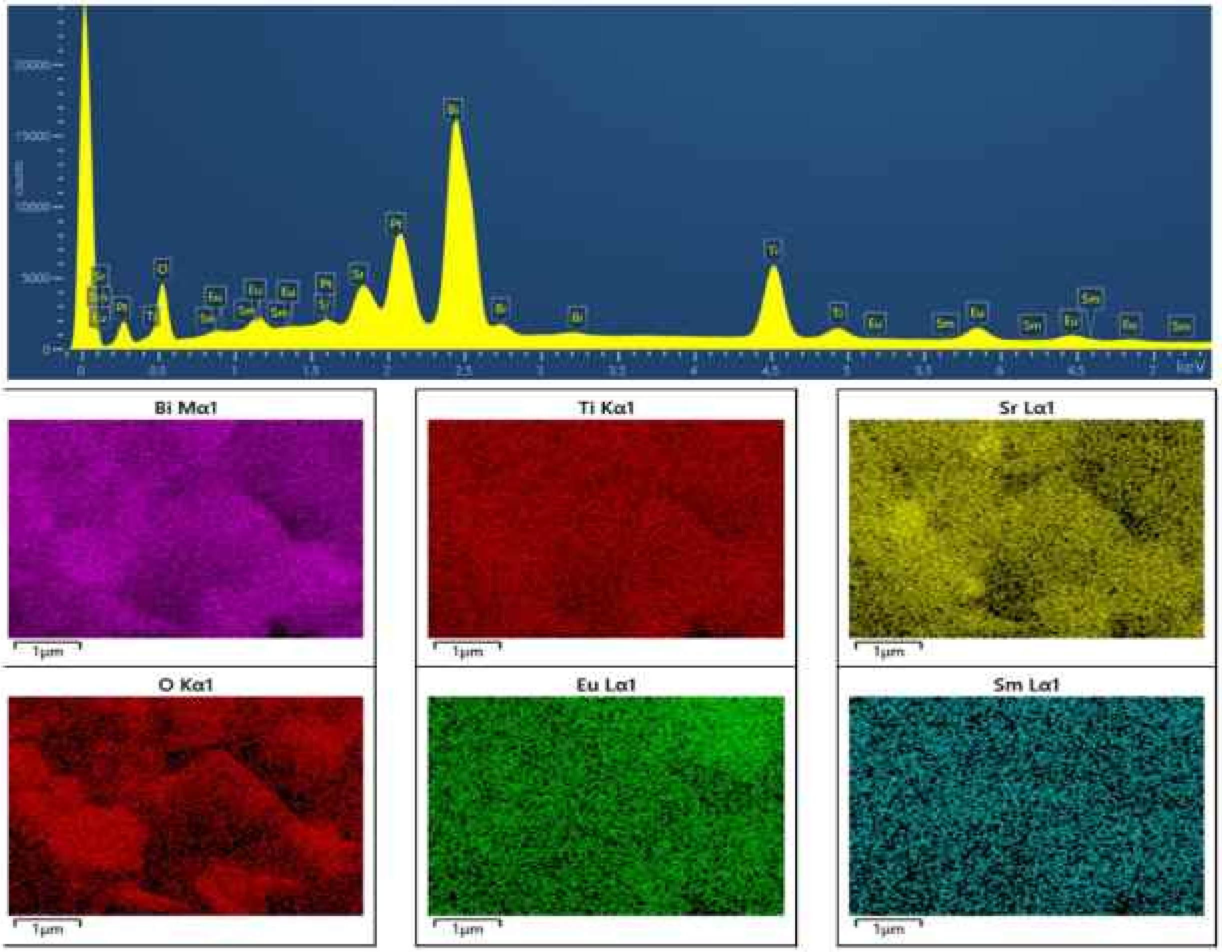


**Fig. 5.** EDX images and elemental mapping results of SBT: $xSm^{3+}/yEu^{3+}$($x = 1$ mol%, $y = 1$mol%) phosphor.

was also indicated by these two distinctive peaks. The symmetric and asymmetric stretching modes of the C—O bond are represented by the absorption peaks of $CO_3^{2-}$ at 1050 and 1490 $cm^{-1}$, respectively [3]. There are two little humps at 2858 and 2931 $cm^{-1}$, which indicates hydrogen bonding [2]. The fundamental O—H stretching vibrations are represented by the absorption band at 3786 $cm^{-1}$.

### 3.4. *Diffuse reflectance spectroscopy*

The DRS spectra of SBT: $xSm^{3+}$ ($x = 1.0$ mol%) and SBT: $xSm^{3+}$, $yEu^{3+}$ ($x = 1.0$mol%, $y = 1.0$, 2.0, 3.0, 4.0, and 5.0 mol%) phosphors are shown in Fig. 7. The charge transfer band transition between $Sm^{3+}$-$O^{2-}$ and $Eu^{3+}$-$O^{2-}$ is represented by the absorption band at 230 nm [19].

The Kubelka-Munk theory was applied to calculate the band gap $E_g$ using the following equations [20,21]:

$$[F(R)h\nu]^{1/n} = A\left(h\nu - E_g\right) \quad (1)$$

$$[F(R)] = \frac{(1-R)^2}{2R} \quad (2)$$

Here, R is the coefficient of reflection and F(R) represents the Kubelka-Munk function. Planck's constant is given by h, ν stands for frequency and c for speed of light. A and n are constants. The sample's characteristics will determine the value of n. For the direct allowed transitions, direct forbidden transitions, indirect allowed transitions, and indirect forbidden transitions, n is given by 1/2, 1/3, 2, or 3 repsectively. An evaluation of the $E_g$ band gap can be made by plotting $[F(R)h\nu]^2$ vs photon energy hν. The $E_g$ band gap for the SBT: 1 mol% $Sm^{3+}$ is 4.59 eV and SBT: $xSm^{3+}/yEu^{3+}$ co-activated phosphors is in the range of 4.70–4.78 eV, as illustrated in Fig. 7 (b&d). This band gap value is comparable to the previously reported band gap values of $Sm^{3+}$ /$Eu^{3+}$ co-doped host lattices. Mukesh K. Sahu et al. reported their work on synthesis and enhancement of photoluminescent properties in spherical shaped $Sm^{3+}/Eu^{3+}$ co-doped $NaCaPO_4$ phosphor particles for w-LEDs and the band gaps for $NaCaPO_4$: $xSm^{3+}$($x = 1.0$ mol%) and $NaCaPO_4$: $xSm^{3+}/yEu^{3+}$ ($x = y = 1.0$ mol%) phosphors were estimated to be about 4.489 and 4.472 eV, respectively [22]. Dongcheng Jiang et al. reported the photoluminescence properties and energy transfer in the $Sm^{3+}$ and $Eu^{3+}$ co-doped $Ca_3Bi(PO_4)_3$ red phosphor and bandgap calculated for CBP: $0.08Sm^{3+}$, $0.05Eu^{3+}$ is 4.04 eV [23]. These band gap values are favourable for the w-LED fabrication.

### 3.5. *Photoluminescence (PL) investigation of single $Sm^{3+}$ and co-doped $Sm^{3+}/Eu^{3+}$ co-doped phosphors*

Fig. 8(a) shows the PL excitation spectrum of SBT: $xSm^{3+}$ ($x = 0.5$mol%) phosphor. The PL excitation spectra of this sample are obtained by monitoring $\lambda_{em} = 600$ nm. Several sharp peaks between 350 and 500 nm can be seen in the spectrum. The peaks at 365, 380, 409, 422, 440, 465 and 481 correspond to transitions from $^6H_{5/2}$ to $^4D_{3/2}$, $^4D_{1/2}$, $^4F_{7/2}$, $^4M_{19/2}$, $^4G_{9/2}$, $^4I_{13/2}$ and $^4I_{11/2}$ respectively. The emission spectra of SBT: $xSm^{3+}$ ($x = 0.5$, 1.0, 1.5 and 2.0mol%) phosphors under 409 nm excitation wavelength have been shown in Fig. 8(b). Four bands at 564, 600, 646 and 708 corresponding to transitions $^4G_{5/2} \rightarrow {}^6H_{5/2}$, $^4G_{5/2} \rightarrow {}^6H_{7/2}$, $^4G_{5/2} \rightarrow {}^6H_{9/2}$, and $^4G_{5/2} \rightarrow {}^6H_{11/2}$ respectively can be observed [24]. PL emission intensity seems to increase till 1.0 mol% of $Sm^{3+}$ ion concentration but decreases beyond that. This can be

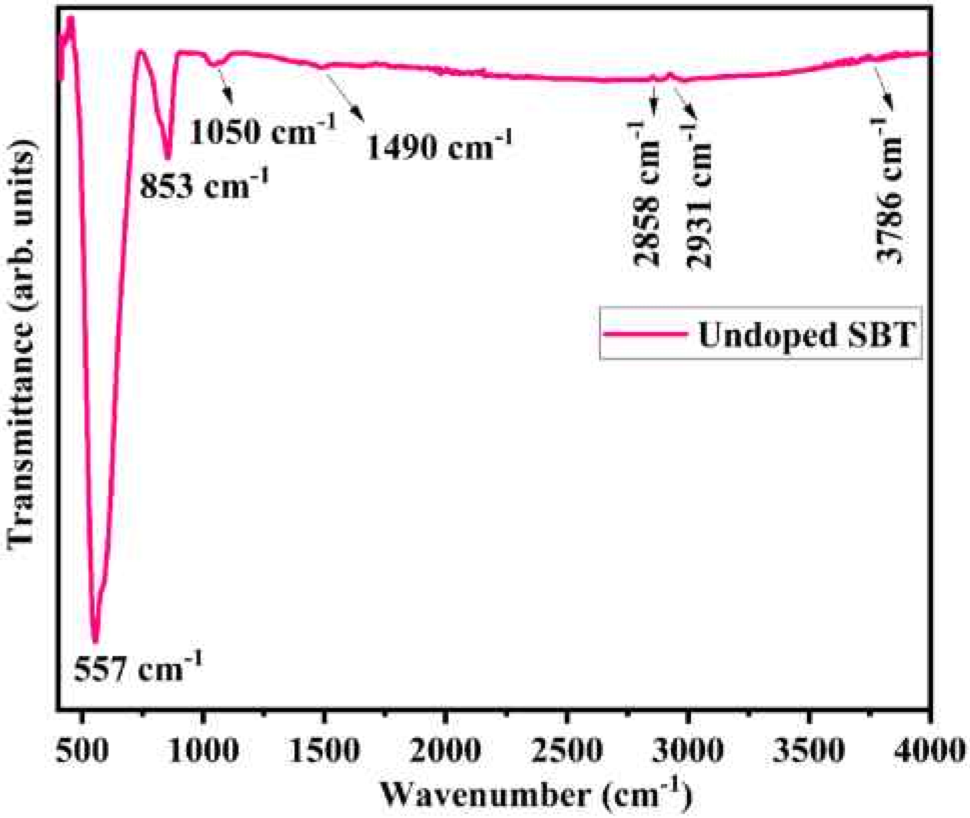


Fig. 6. FTIR spectra of un-doped SBT phosphor.

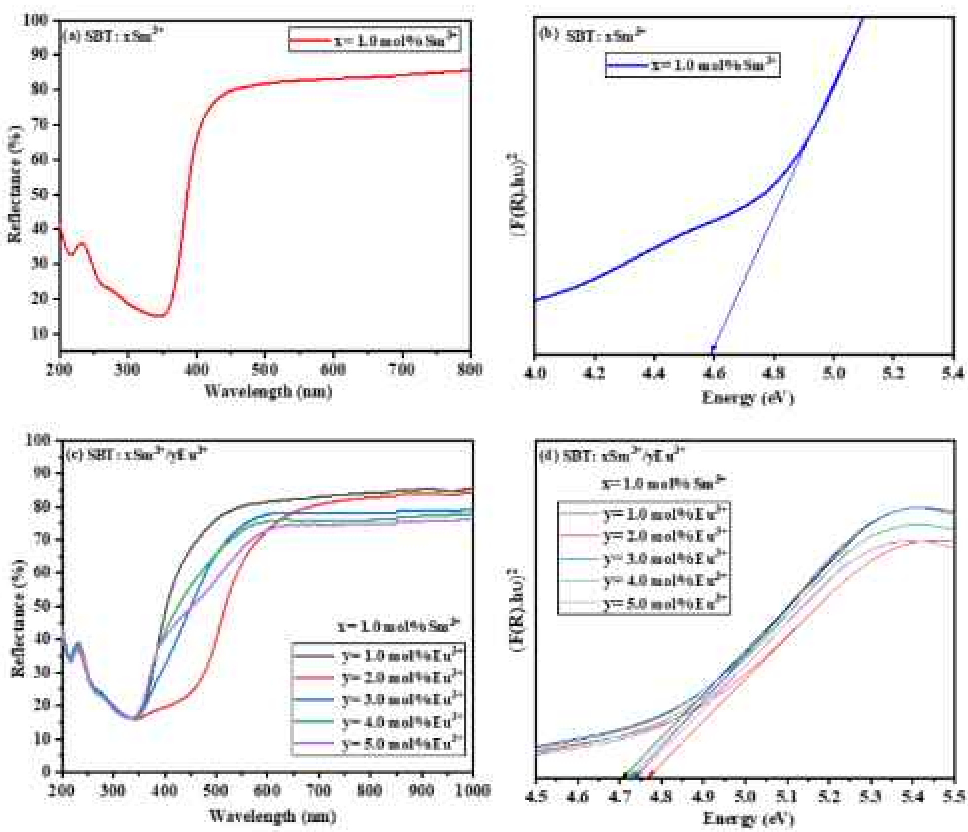


Fig. 7. DRS spectra of SBT: $xSm^{3+}(x = 1$ mol%) and SBT: $xSm^{3+}/yEu^{3+}(x = 1$ mol%, $y = 1,2,3,4$ and 5mol%) phosphor.

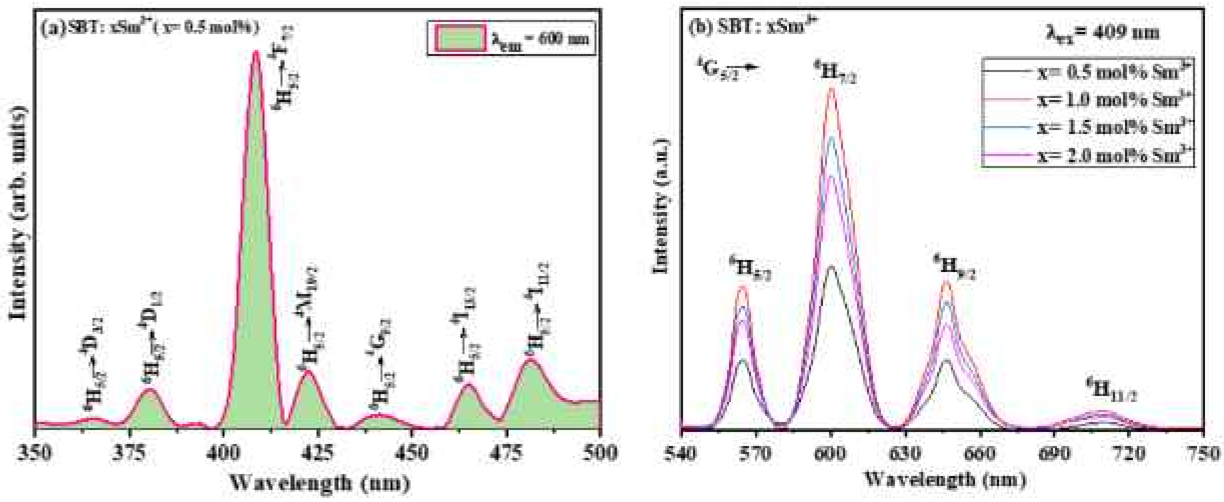


**Fig. 8.** PL excitation spectrum (a) of SBT: $xSm^{3+}$ ($x = 0.5$mol%) phosphor and emission spectra (b) of SBT: $xSm^{3+}$ ($x = 0.5$, 1.0, 1.5 and 2.0mol%) phosphors.

attributed to the phenomenon of concentration quenching wherein the activator ions undergo non-radiative losses due to excessive ions in each other's vicinity.

Fig. 9 illustrates the excitation and emission spectra of SBT: $yEu^{3+}$ ($y = 1$ mol%) phosphor. The excitation spectrum, recorded at $\lambda_{em} = 615$ nm, comprises peaks at 353, 396 and 465 nm corresponding to the transitions from excited state $^7F_0$ to the $^5D_4$, $^5L_6$ and $^5D_2$ emission states of $Eu^{3+}$ respectively. The emission spectra were recorded in the wavelength range 560–760 nm on pumping the phosphor at three different excitation wavelengths $\lambda_{ex} = 353$, 396 and 465 nm. Peaks at 593, 615, 652 and 703 nm owning to transitions $^5D_0 \rightarrow {}^7F_1$, $^5D_0 \rightarrow {}^7F_2$, $^5D_0 \rightarrow {}^7F_3$ and $^5D_0 \rightarrow {}^7F_4$ respectively were observed [25]. Out of these peaks, the one at 615 nm was the most intense and the highest emission intensity was observed at $\lambda_{ex} = 353$ nm wavelength.

Fig. 10 (a, b & c) illustrates the comparison of emission spectra of singly $Eu^{3+}$ doped SBT: $yEu^{3+}$ ($y = 1.0$ mol%) and co-doped SBT: $xSm^{3+}/yEu^{3+}$ ($x = 1.0$ mol%, 1.0 mol%) phosphors under three different excitations, $\lambda_{ex} = 353$, 396 and 465 nm respectively. Higher luminescence intensity for $Sm^{3+}/Eu^{3+}$ co-activated phosphors can be seen as compared to single $Eu^{3+}$ ion activated phosphors. This shows that energy transfer takes place from $Sm^{3+}$ to $Eu^{3+}$ ions due to which emission intensity increases multiple times. Co-doping with an activator ion increases the absorption cross-section and subsequently enhances luminescence efficiency. Since there is a very small energy difference between the energy level $^4G_{5/2}$ of the $Sm^{3+}$ ion and the $^5D_0$ level of the $Eu^{3+}$ ion, $Sm^{3+}$ act as an efficient sensitizer and transfers its energy to $Eu^{3+}$ ions which in results in enhanced luminescence. Energy transfer between $Sm^{3+}$ and $Eu^{3+}$ ions can tune the luminescent colour of the

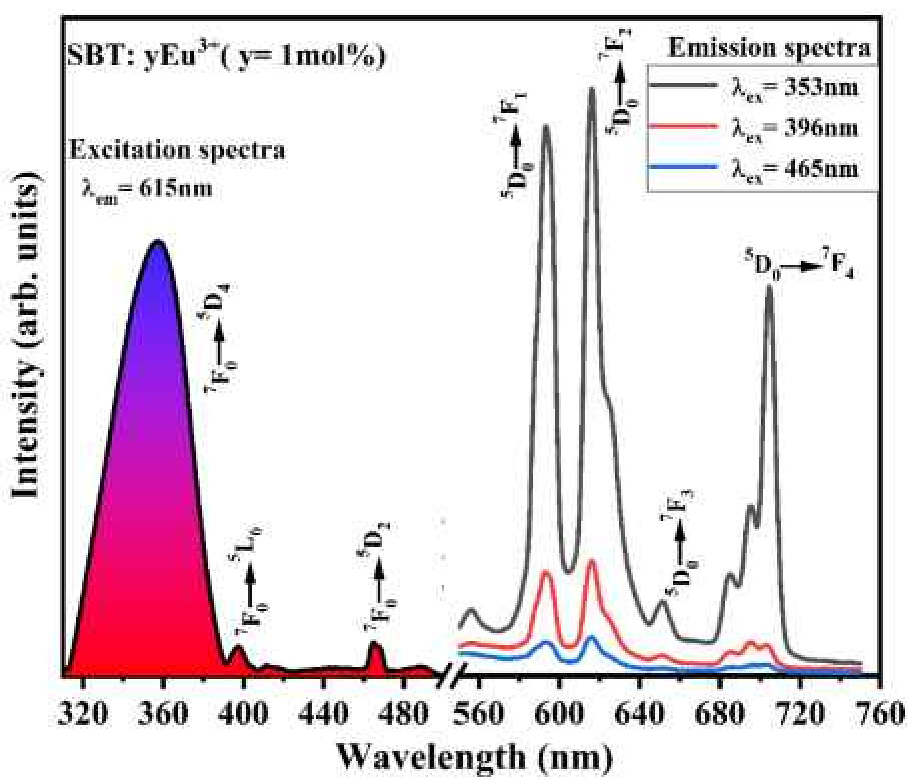


**Fig. 9.** Excitation and emission spectra of SBT: $yEu^{3+}$ ($y = 1$ mol%) phosphor.

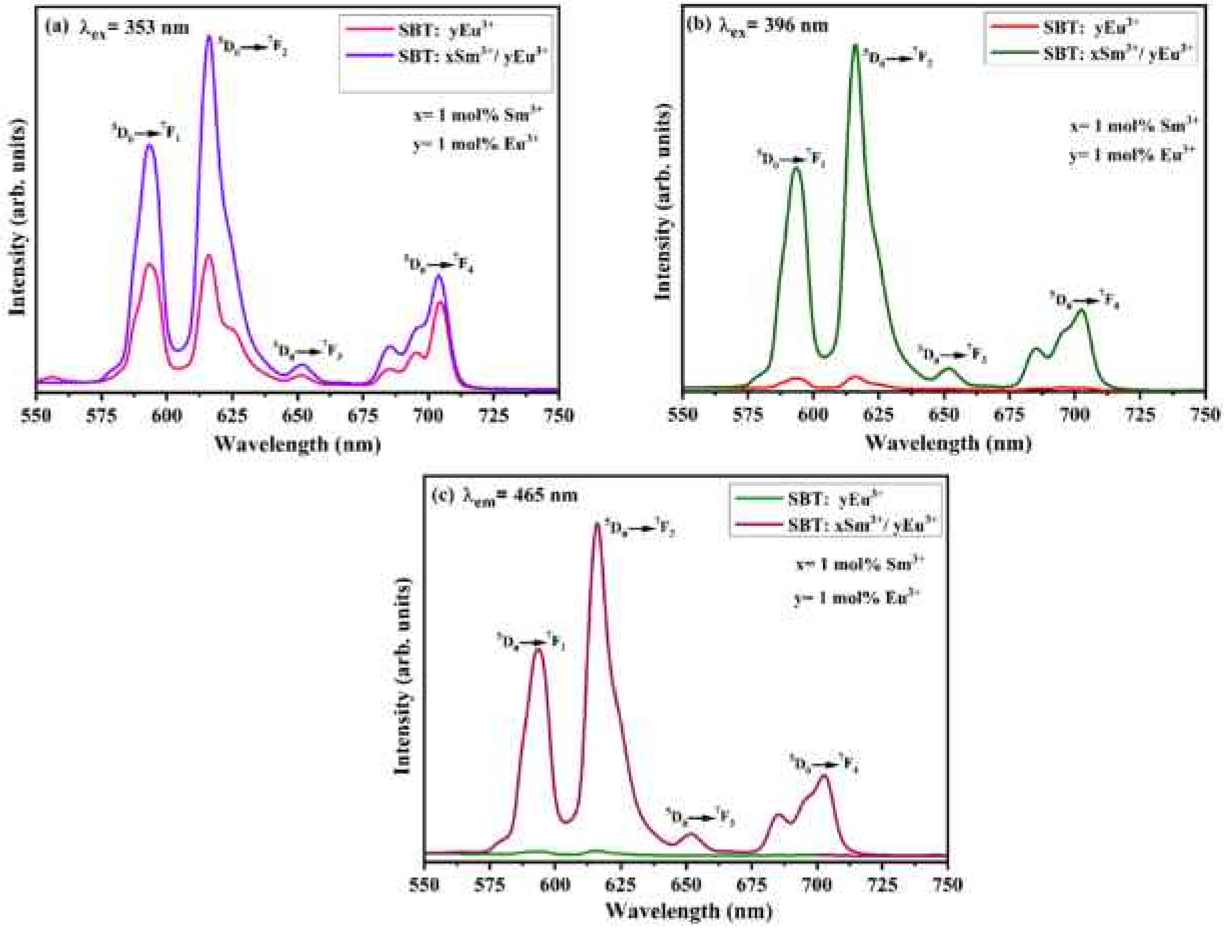


**Fig. 10.** (a, b & c). Comparison of emission spectra of SBT: $yEu^{3+}$ ($y = 1.0$ mol%) and co-doped SBT: $xSm^{3+}/yEu^{3+}$ ($x = 1.0$ mol%, 1.0 mol%) phosphors.

phosphor. This is especially important in LED applications where different light sources or applications require specific colours. The combination of $Sm^{3+}$ and $Eu^{3+}$ ions helps achieve better color rendering index (CRI) in LED lighting. The high color rendering index makes the illuminated object look natural and vibrant. The electron exchange process between $Sm^{3+}$ and $Eu^{3+}$ ions can achieve energy conversion, enabling the LED to emit increasingly brighter light.

Emission spectra of SBT: $xSm^{3+}/yEu^{3+}$ ($x = 1$mol%, $y = 1, 2, 3, 4$ and 5mol%) have been shown in Fig. 11(a, b, c & d). The spectra were recorded at four different excitation wavelengths 353, 396, 409 and 465 nm respectively. The spectra comprise of several peaks at positions 593, 615, 652 and 703 nm owing to transitions $^5D_0 \rightarrow {}^7F_1$, $^7F_2$, $^7F_3$, and $^7F_4$ respectively. It can be clearly seen that increasing $Eu^{3+}$ concentration results in increase in emission intensity up to 2 mol% of $Eu^{3+}$ ions. After that, emission intensity decreases gradually. That means 1.0 mol% of $Sm^{3+}$ ion concentration in singly $Sm^{3+}$ activated phosphors and 2 mol% of $Eu^{3+}$ ion concentration in co-activated phosphors is the optimum concentration of RE ions for this particular host lattice. Fig. 12 shows the energy level diagram showing various transitions exhibited by $Sm^{3+}$ and $Eu^{3+}$ ions [26–28].

Dexter's theory was applied along with Reisfeld's approximation, to check the type of multipolar interaction by using the given equation -

$$\frac{I_{S0}}{I_{SU}} \alpha\, C^{n/3}$$

where $I_{S0}$ and $I_{SU}$ are the luminescence intensities of the SBT: $Sm^{3+}/Eu^{3+}$co-doped phosphor with the absence and presence of $Eu^{3+}$ ions respectively. C is the sum of the concentration of $Sm^{3+}$ and $Eu^{3+}$; $n = 6$, 8, 10 represent dipole–dipole ($d - d$), dipole–quadrupole ($d - q$), and quadrupole–quadrupole ($q - q$) interactions, respectively. Fig. 13 shows the linear regression between $I_{S0}/ I_{SU}$ versus $C^{n/3}$. The best linear fit was observed for $n = 8$, means the type of interaction involved here is dipole-quadrupole interaction.

### 3.6. Quantum yield

To assess the quantitative emission performance of the phosphor the quantum yield (QY) measurement was done using Horiba QuantaPhi-2 integrating sphere. The scattered 396 nm excitation spectra (Rayleigh Spectra) were recorded for both the blank cup ($R_b$), and the optimized sample (SBT: $xSm^{3+}/yEu^{3+}$, $x = 1.0$mol%, $y = 2$ mol%) ($R_s$). Integration of instrument corrected Rayleigh intensities was performed from 386 nm to 406 nm as shown in Fig. 14(a).

Thereafter, the fluorescence emission for blank and sample were measured and integration of the emission signals $E_b$ (blank) and $E_s$ (sample) was performed from 550 nm to 750 nm as shown in Fig. 14(b).

The quantum Yield (Φ) is estimated using the following relation:

$$(\Phi) = 100\% \times \frac{[E_s - E_b]}{R_b - R_s}$$

Since the integration time constant used to collect the $E_b$, and $E_s$ was 8 time longer than for $R_b$ and $R_s$ during the measurement so the difference $E_s$ -$E_b$ is divided by 8 in the equations.

The QY of the optimal sample SBT:1 mol% $Sm^{3+}$, 2 mol% $Eu^{3+}$ is calculated as 58.9 which is relatively higher than the previous literature values reported for $Sr_3Y(BO_3)_3$:$0.07Sm^{3+}$, $0.15Eu^{3+}$ (38.7 %) [29], $Sr_9Y_2W_4O_{24}$:$0.02Sm^{3+}$/0.05mol% $Eu^{3+}$ (51.2 %) [30], $NaLa_{0.65}MgWO_6$:$0.05Sm^{3+}$·$0.3Eu^{3+}$ (48 %) [31] phosphors. This high

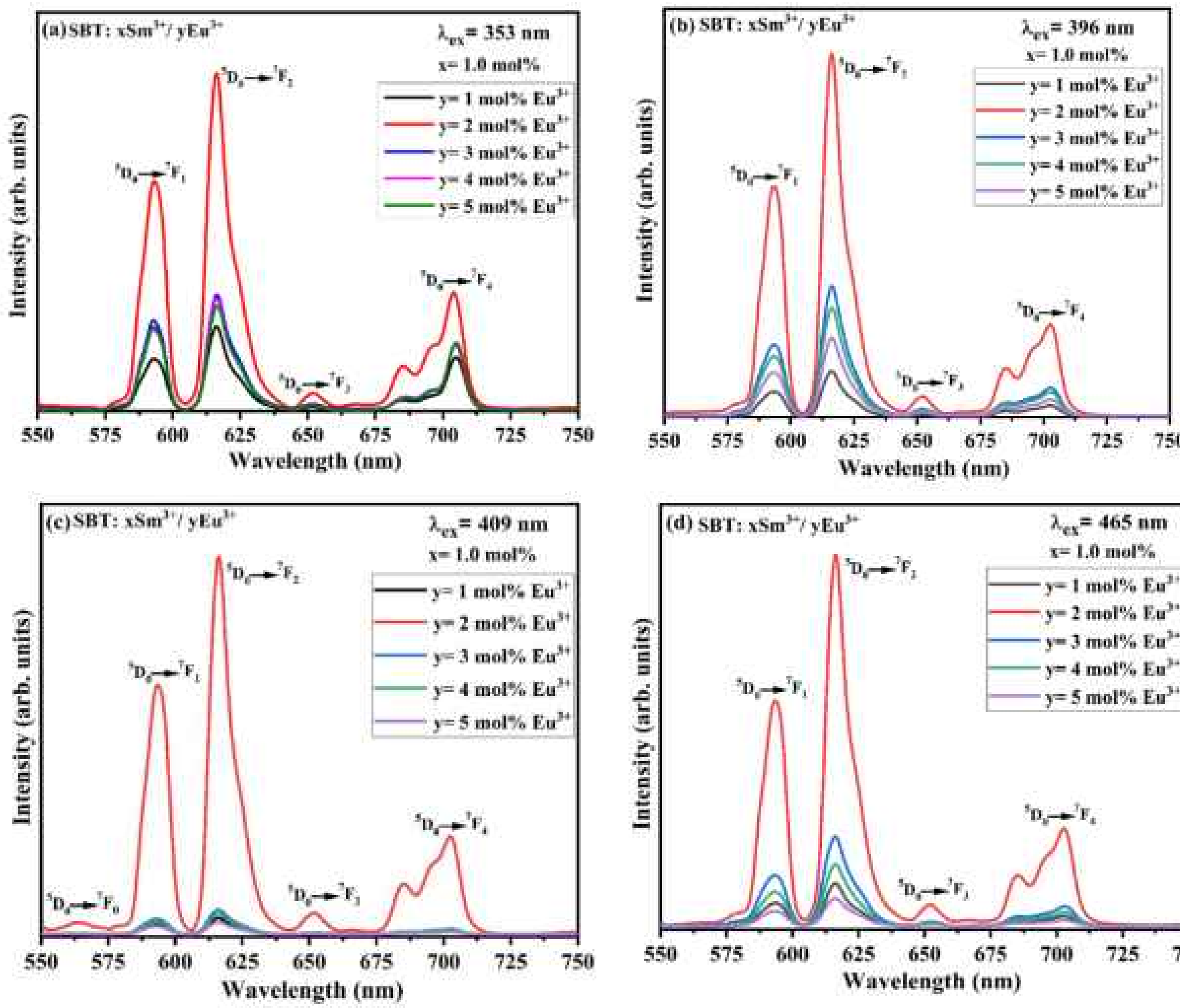


Fig. 11. (a, b, c & d). $Eu^{3+}$ concentration dependent emission spectra of SBT: $xSm^{3+}/yEu^{3+}$ ($x = 1$mol%, $y = 1, 2, 3, 4$ and 5mol%).

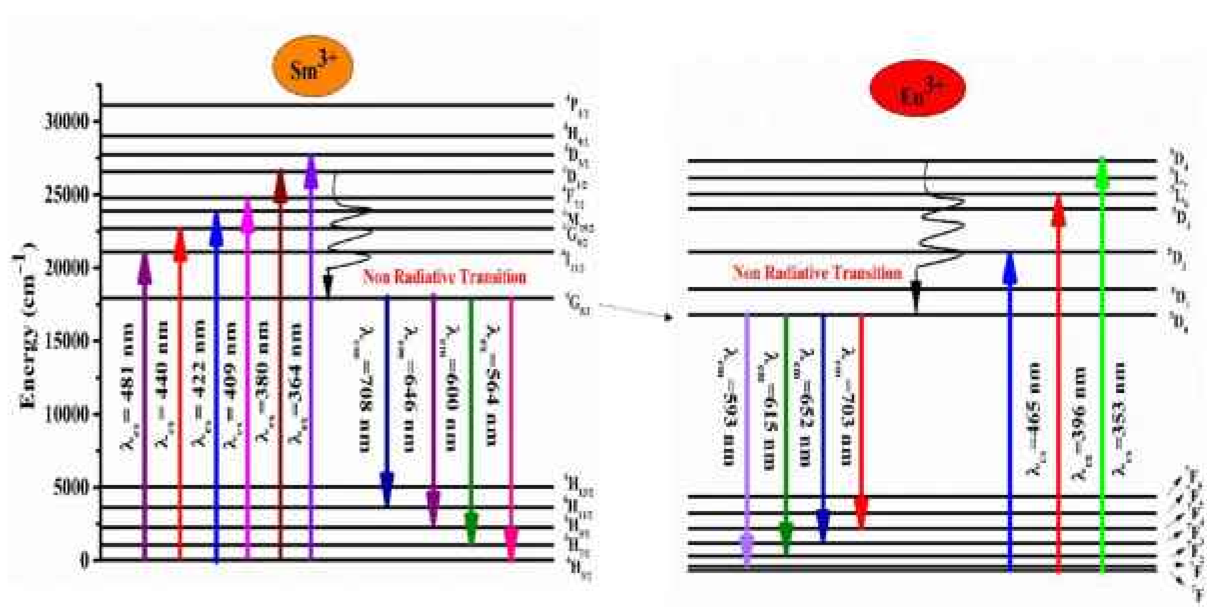


Fig. 12. Energy level diagram showing various transitions exhibited by $Sm^{3+}$ and $Eu^{3+}$ ions.

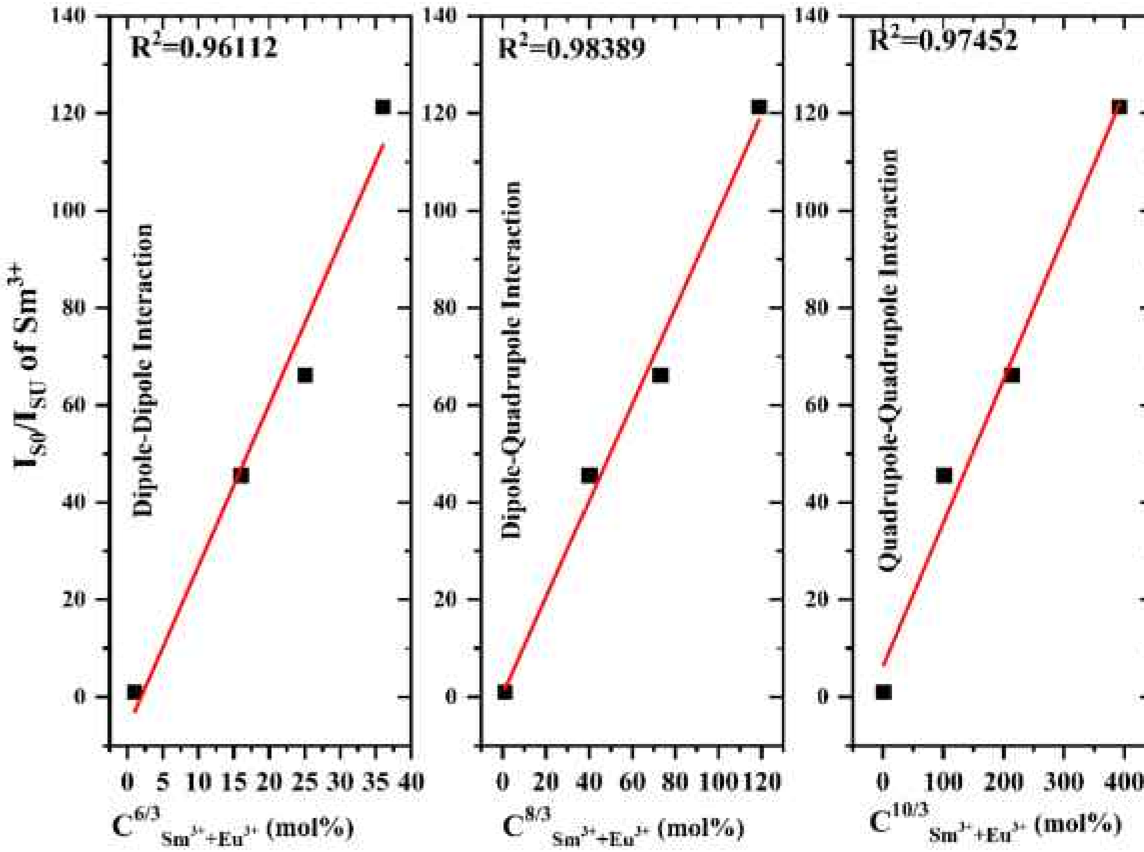


**Fig. 13.** Variation of $I_{S0}/I_{SU}$ of $Sm^{3+}$ ion w.r.t. $C^{6/3}$, $C^{8/3}$ and $C^{10/3}$ for SBT: $xSm^{3+}/yEu^{3+}$ ($x = 1.0$mol%, $y = 1, 2, 3, 4$ and 5mol%) co-doped phosphors under 409 nm excitation wavelength.

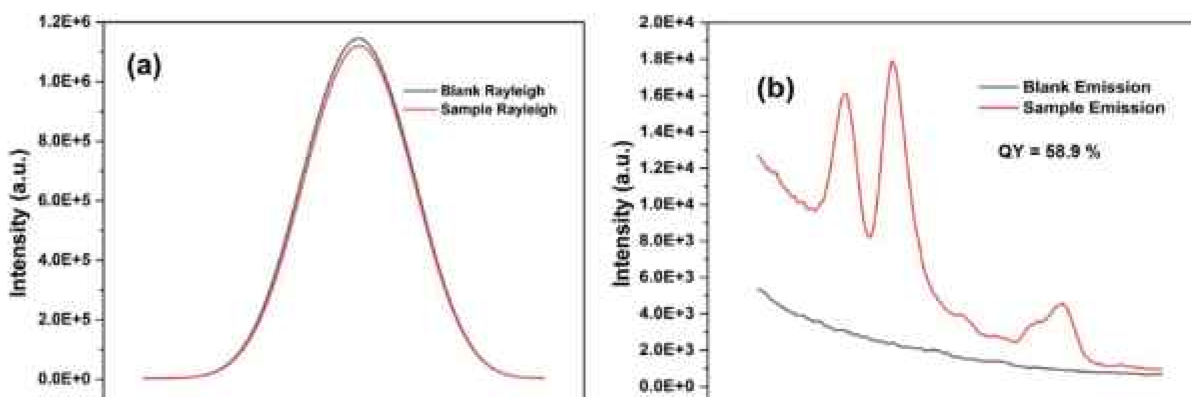


**Fig. 14.** Determination of quantum yield for SBT: $xSm^{3+}/yEu^{3+}$ ($x = 1.0$mol%, $y = 2$ mol%) phosphor.

QY result allows us to consider the use of the above phosphor in the application of photonic devices.

### 3.7. PL decay curves

Fig. 15 shows the SBT: $xSm^{3+}$ /$yEu^{3+}$ co-doped phosphors' normalised PL decay curves at 409 nm excitation wavelength. A double-exponential function using the following formula was used to fit the decay curves [32]:

$$I = I_0 + B_1\ exp.\left(\frac{-t}{\tau_1}\right) + B_2\ exp.\left(\frac{-t}{\tau_2}\right) \tag{3}$$

Where $I_o$ and I represent the intensities at time 0 and after t seconds, respectively; $B_1$ and $B_2$ are the fitting constants and $\tau_1$ and $\tau_2$, respectively stand for the fast and slow decay time components. The average phosphor lifespan is calculated using the relation shown below [33]:

$$\tau_{avg.} = \frac{A_1\tau_1^2 + A_2\tau_2^2}{A_1\tau_1 + A_2\tau_2} \tag{4}$$

The calculated lifetime values of the co-doped phosphors are listed in Table 1. The lifetimes values decrease with increasing $Eu^{3+}$ concentration thereby implying an effective energy transfer from $Sm^{3+}$ to $Eu^{3+}$ ions [34].

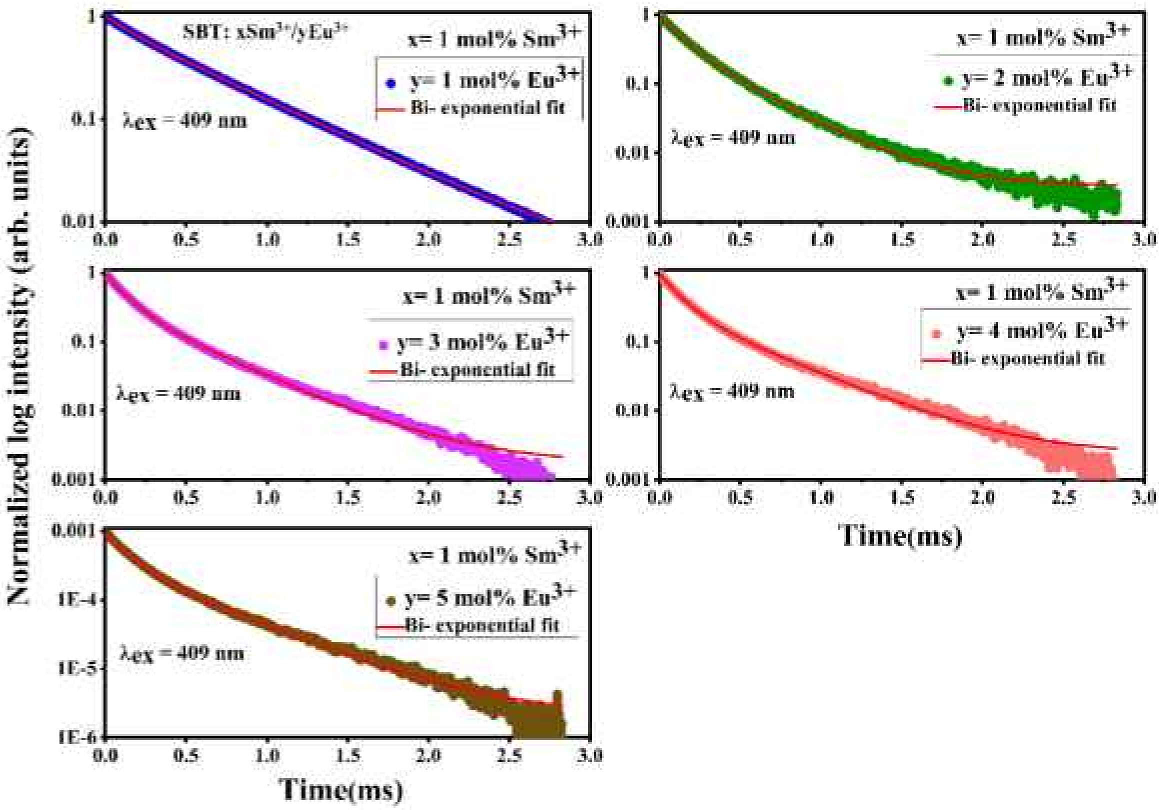


**Fig. 15.** PL decay curves of SBT: $xSm^{3+}/yEu^{3+}$ co-doped phosphors at 409 nm excitation wavelength.

**Table 1**
Lifetime decay values of SBT: $xSm^{3+}/yEu^{3+}$ co-doped phosphors.

| Sample ID ($xSm^{3+}/yEu^{3+}$series) | Lifetime values (ms) |
|---|---|
| $x = 1.0$mol%, $y = 1$ mol% | 5.68 |
| $x = 1.0$mol%, $y = 2$ mol% | 2.77 |
| $x = 1.0$mol%, $y = 3$ mol% | 3.13 |
| $x = 1.0$mol%, $y = 4$ mol% | 3.27 |
| $x = 1.0$mol%, $y = 0$ mol% | 3.57 |

### 3.8. *Colorimetric analysis*

The optimal $Sm^{3+}$ doped and $Sm^{3+}/Eu^{3+}$ co-doped SBT phosphors' chromaticity diagrams from the Commission Internationale de l'éclairage (CIE) are shown in Fig 16. The emission spectra of $Sm^{3+}$ doped phosphors that was recorded at excitation wavelength 409 nm and $Sm^{3+}/Eu^{3+}$ co-doped phosphors that were recorded at excitation wavelengths 353, 396, and 409 nm, respectively, were used to calculate CIE points. The CIE coordinates of optimized $Sm^{3+}$ion doped phosphor fall in orange-reddish region. From Fig. 16, we can find that CIE co-ordinates for $Sm^{3+}/Eu^{3+}$ ion co-doped SBT phosphors shifted from orange-reddish to deep red region. Thus, the CIE co-ordinates show a color tunability in $Sm^{3+}/Eu^{3+}$ co-activated phosphors as compared to singly doped $Sm^{3+}$ activated SBT phosphors. Color tunability allows users to adjust the lighting environment to their preferences and specific needs. This change is beneficial in creating different climates in residential, commercial and industrial areas. Adjustable LED lighting can be used to simulate natural day changes, support circadian rhythms and promote better sleep. In medical facilities, lighting can be adjusted according to the comfort and health of the patient [35]. This capability opens up new possibilities in various fields, enabling the customization of lighting and display technologies to meet specific requirements and enhance visual experiences.

Correlated colour temperature (CCT) is an additional important parameter for illustrating the suitability and importance of $RE^{3+}$ doped phosphor. The CCT represents the colour hue of a light source emitted from a phosphor when it is excited by an energy source. With the use of the empirical McCamy equation, the CCT values was computed [36]:

$$CCT = -449n^3 + 352n^2 - 6823.3n + 5520.33 \quad (5)$$

Where (x, y) is the CIE coordinate, $(x_e, y_e)$ is the chromaticity epicentre with coordinates (0.338, 0.186), and $(x_e, y_e)$ is the chromaticity epicentre, and $n = (x\text{-}x_e)/(y\text{-}y_e)$ is the inverse slope line. Table 2 contains a list of the calculated CCT values and CIE coordinates.

### 3.9. *Temperature dependent PL (TDPL)*

Temperature dependent PL is an essential characterisation technique to assess the thermal stability of the as prepared phosphor especially if such materials are being targeted for usage in w-LEDs and other lighting applications where operating temperatures are very high. Here, the temperature-dependent emission spectra of a $xSm^{3+}/yEu^{3+}$ ($x = 1.0$mol %, $y = 2$ mol%) co-doped SBT phosphor were recorded in the temperature range of 298 to 423 K at intervals of 25 K under 409 nm excitation (Fig. 17a). The spectra show that the thermal quenching effect causes the emission intensity to steadily decrease as temperature rises. The intensity measured at 298 K decreased by 72 percent at 398 K, showing that the synthesised co-doped phosphors had some thermal stability and might be used to create effective lighting and display systems. Additionally, the Arrhenius relation can be used to compute the activation energy (ΔE), which is a crucial quantity to determine the thermal stability of the phosphors [37,38].

$$I_T = \frac{I_0}{1 + C\,exp.\left(\frac{\Delta E}{K_BT}\right)} \quad (6)$$

Here, C is a constant and K is the Boltzmann's constant, $I_0$ is the PL

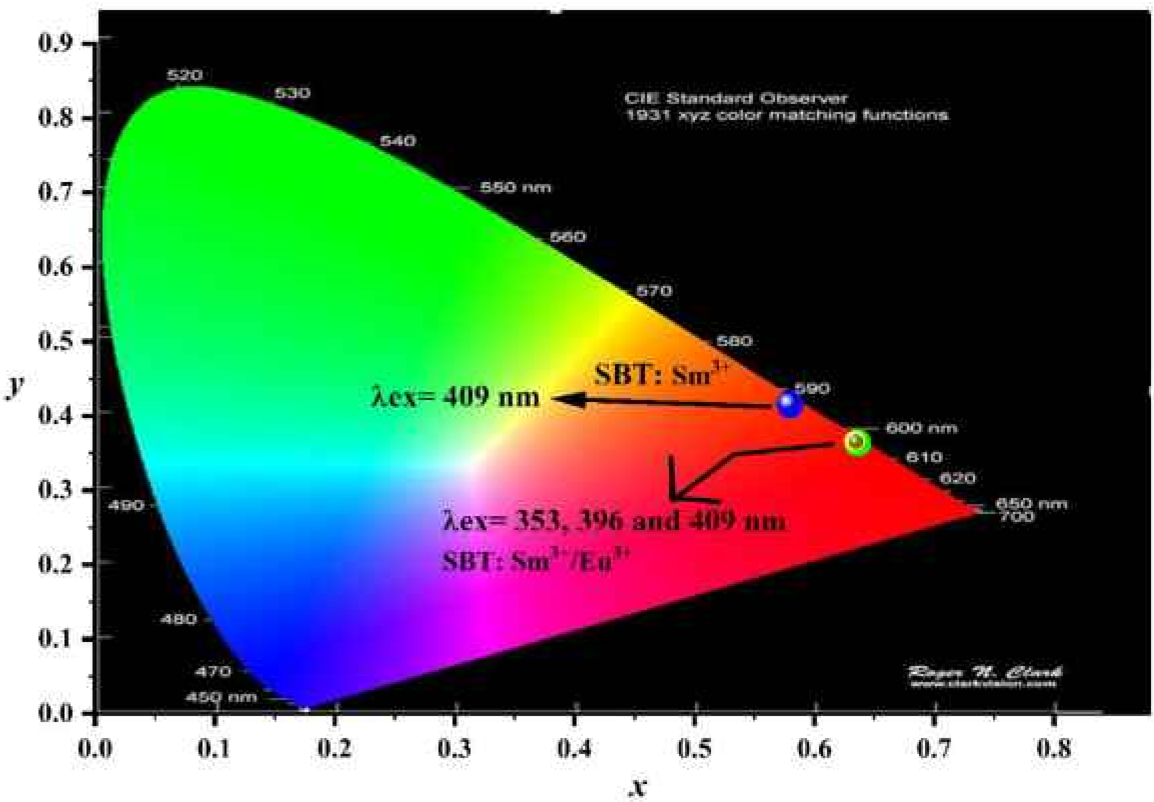


**Fig. 16.** CIE co-ordinates of optimal $Sm^{3+}$ doped and $Sm^{3+}/Eu^{3+}$ co-doped SBT phosphors.

**Table 2**
Variations of CIE Coordinates and CCT values for optimized singly $Sm^{3+}$ ion doped and co doped $Sm^{3+}/Eu^{3+}$ SBT phosphor.

| Sample ID ($xSm^{3+}/yEu^{3+}$series) | $\lambda_{ex}$ | CIE Co-ordinates | CCT(K) |
|---|---|---|---|
| $x = 1.0$mol%, $y = 0$ mol% | 409 nm | (0.579, 0.415) | 1765 |
| $x = 1.0$mol%, $y = 2$ mol% | 353 nm | (0.635, 0.365) | 2106 |
| $x = 1.0$mol%, $y = 2$ mol% | 396 nm | (0.636, 0.363) | 2136 |
| $x = 1.0$mol%, $y = 2$ mol% | 409 nm | (0.634, 0.366) | 2081 |

intensity at 298 K and $I_T$ is the intensity at various testing temperatures. The slope of graph $Ln[(I_0/I_T) - 1]$ vs. $1/K_BT$ shown in Fig 17(b) can be used to determine the value of ΔE. As a result, ΔE calculated value is 0.385 eV which is relatively higher than the previously reported values for $Ba_3MoTiO_8$:$xSm^{3+}/yEu^{3+}$ ($x = 1.5$ mol%, $y = 4$ mol%) (ΔE=0.306) [37], $Sr_9Y_2W_4O_{24}$: $xSm^{3+}/yEu^{3+}$($x = 2$ mol%, $y = 5$ mol%) (ΔE=0.306) [30], $Zn_{0.99-y}Nb_2O_6$: $0.01Sm^{3+}$, $0.25Eu^{3+}$(ΔE=0.235) [39]. Higher activation energy generally corresponds to a slower reaction rate. Substances with higher activation energy can withstand higher temperatures without undergoing significant chemical changes because the thermal energy available at those temperatures may not be sufficient to overcome the activation energy barrier.

## 4. Conclusion

In conclusion, the current paper presents morphological and photoluminescent analysis of $Sm^{3+}$/ $Eu^{3+}$ co-doped SBT phosphors produced using a typical solid-state reaction approach. Studies have been done on the structural, optical, and thermal stability of as prepared phosphors. All phosphors have orthorhombic crystal structures, which is confirmed by the XRD investigation. FT-IR analysis gave information about the vibrational states and functional groups present in the lattice of the phosphors. From the UV–Vis-NIR absorption investigation, it was seen that the band gap of the phosphors changes after doping with rare earth ions possibly as a result of the development of extra trap states in the conduction and valance band region. PL emission and excitation studies on singly doped $Sm^{3+}$ SBT phosphors were conducted at 409 ($^6H_{5/2} \rightarrow {}^4F_{7/2}$) nm excitation and 600 nm ($^4G_{5/2} \rightarrow {}^6H_{7/2}$) emission wavelengths, respectively. PL excitation and emission investigations on $Sm^{3+}/Eu^{3+}$ co-doped phosphors were also recorded at various excitation wavelengths ($\lambda_{ex}$=353, 396, and 409 nm). Energy transfer from $Sm^{3+}$ to $Eu^{3+}$ ions inside the host lattice was studied by comparing the emission spectra of $Sm^{3+}$ and $Sm^{3+}/Eu^{3+}$ co-activated phosphors. Using temperature dependent PL analysis, the thermal stability of the phosphors was investigated in the temperature range of 298–423 K. After $Eu^{3+}$ co-doping in $Sm^{3+}$ doped phosphors, a considerable shift in the CIE co-ordinates from the reddish-orange to the pure red region was seen. As a result, our research supports the idea that $Sm^{3+}$ and $Eu^{3+}$ co-doped SBT phosphors, when used in the right proportions, can trigger efficient energy transfer phenomena and can be used as deep red emitting component of w-LEDs and in thermally stable lighting and display technologies.

## CRediT authorship contribution statement

**Pooja Rohilla:** Writing – original draft, Visualization. **Sheetal Kumari:** Writing – review & editing, Software, Investigation. **Ravita:** Investigation, Formal analysis. **Samarthya Diwakar:** Visualization, Methodology. **Rupesh Talewar:** Investigation. **Ankur Shandilya:** Investigation. **Kartika Maheshwari:** Investigation. **M. Venkateswarlu:** Formal analysis. **Aman Prasad:** Validation, Supervision, Funding acquisition, Data curation. **A.S. Rao:** Supervision, Conceptualization.

## Declaration of competing interest

The authors declare that they have no known competing financial interests or personal relationships that could have appeared to influence the work reported in this paper.

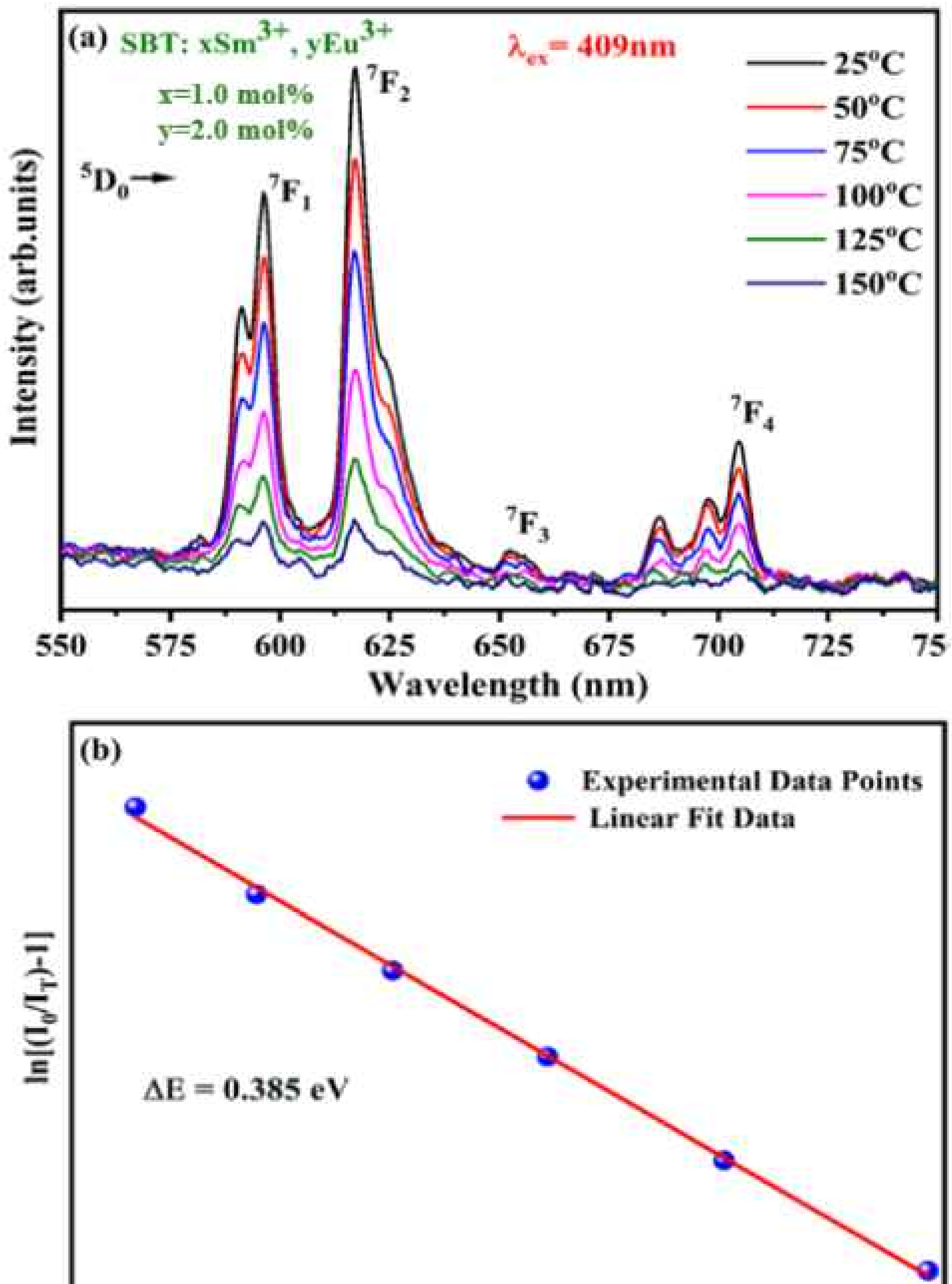


**Fig. 17.** (a). Temperature dependent PL spectra of SBT: $xSm^{3+}/yEu^{3+}$ ($x = 1.0$mol%, $y = 2$ mol%) phosphor. (b). $Ln[(I_0/I_T) -1]$ vs. $1/K_BT$ plot for activation energy.

**Data availability**

The data that support the findings of this study are available on request from the corresponding author Dr. Aman Prasad. The data are not publicly available due to restrictions, e.g. their containing information that could compromise the privacy of research participants.

*Acknowledgement*

Dr. Aman Prasad is grateful to Dayalbagh Educational Institute (DEI), Deemed University, Agra for providing a Research Seed Money Grant (DEI/GBMF(3052022)/518). We are also really grateful To Dr. Shayama Prasad and Dr. Manju Srivastava in the Department of Chemistry at Dayalbagh Educational Institute (DEI), Deemed University, Agra for making the FESEM facility available to us.

**References**

[1] S.G.M. Mushtaque, A.R. Kadam, S.J. Dhoble, High color purity and color tunability in $Sm^{3+}/Eu^{3+}$ activated /co-activated $Sr_6Ca_4(PO_4)_6F_2$ phosphor for WLED and display devices application, J. Mol. Struct. 1274 (2023) 134510, https://doi.org/10.1016/j.molstruc.2022.134510.

[2] R. Kokate, P. Rohilla, S. Kaur, A.S. Rao, V. Singh, Visible emission characteristics in $Tb^{3+}$-doped $KNa_3A_{l4}Si_4O_{16}$ phosphor, Optik 243 (2021) 167391, https://doi.org/10.1016/j.ijleo.2021.167391.

[3] V. Singh, P. Rohilla, S. Kaur, A.S. Rao, Optik $Tb^{3+}$ activated $Na_3YSi_2O_7$ phosphors for display panels, Optik 271 (2022) 170221, https://doi.org/10.1016/j.ijleo.2022.170221.

[4] B. Po, A high color purity red-emission phosphor based on $Sm^{3+}$ and $Eu^{3+}$ co-doped $Ba_3(Po_4)$, Mater. Res. Bull. 126 (2020) 110836, https://doi.org/10.1016/j.materresbull.2020.110836.

[5] P.K. Pandey, P. Dixit, V. Chauhan, P.C. Pandey, Luminescence properties and energy transfer studies in thermally stable $Bi_2O_3$ :$Sm^{3+}$, $Eu^{3+}$ phosphor, J. Alloys Compd. 952 (2023) 169911, https://doi.org/10.1016/j.jallcom.2023.169911.

[6] Y. Zhang, J. Xu, Q. Cui, B. Yang, $Eu^{3+}$ -doped $Bi_4Si_3O_{12}$ red phosphor for solid state lighting: microwave synthesis, characterization, photoluminescence properties and thermal quenching mechanisms, Sci. Rep. 7 (2017) 1–12, https://doi.org/10.1038/srep42464.

[7] S. Dong, S. Ye, L. Wang, X. Chen, S. Yang, Y. Zhao, J. Wang, X. Jing, Q. Zhang, $Gd_2B(W,Mo)O_9$: $Eu^{3+}$ red phosphor: from structure design to photoluminescence behavior and near-UV white-LEDs performance, J. Alloys Compd. 610 (2014) 402–408, https://doi.org/10.1016/j.jallcom.2014.05.011.

[8] D. Poelman, P. Smet, Europium-doped phosphors for lighting: the past, the present and the future, Int. Work. Adv. Nanovision Sci. (2011) 18–21. http://hdl.handle.net/1854/LU-1235812.

[9] L. Yu, J. Hao, Z. Xu, W.E.I. Li, R. Chu, Strong photoluminescence and improved electrical properties in Eu-modified $SrBi_4Ti_4O_{15}$ Multifunctional Ceramics, J. Electron. Mater. 46 (2017) 4398–4404, https://doi.org/10.1007/s11664-017-5427-7.

[10] T. Wei, F. Yang, B. Jia, C. Zhao, M. Wang, M. Du, Q. Zhou, Y. Guo, Z. Li, High performance temperature sensing and optical heating of $Tm^{3+}$ - and $Yb^{3+}$ -codoped $SrBi_4Ti_4O_{15}$ up-conversion luminescence nanoparticles, Ceram. Int. 45 (2019) 18084–18090, https://doi.org/10.1016/j.ceramint.2019.06.030.

[11] Y. Zhang, L. Duan, A. Zhang, D. Wang, R. Chu, Z. Xu, G. Li, C. Zhang, Photoluminescence, electrical properties and electron band structure of $(Ho, Yb)^{3+}$ co-doped $SrBi_4Ti_4O_{15}$ multifunctional ceramics, Ceram. Int. 48 (2022) 9248–9257, https://doi.org/10.1016/j.ceramint.2021.12.111.

[12] H. Zou, Y. Hu, X. Zhu, Y. Sui, X. Wang, Z. Song, Photoluminescence, enhanced ferroelectric and dielectric properties of $Pr^{3+}$ doped $SrBi_4Ti_4O_{15}$ multifunctional ceramics, Ferroelectrics 488 (2015) 62–70, https://doi.org/10.1080/00150193.2015.1102004.

[13] Y. Wu, X. Zhao, Z. Zhang, J. Xiang, H. Suo, C. Guo, Dual-mode dichromatic $SrBi_4Ti_4O_{15}$: $Er^{3+}$ emitting phosphor for anti-counterfeiting application, Ceram. Int. 47 (2021) 15067–15072, https://doi.org/10.1016/j.ceramint.2021.02.064.

[14] T. Wei, F. Yang, Q. Jing, C. Zhao, M. Wang, M. Du, Y. Guo, Q. Zhou, Z. Li, Optical multi-functionalities of $Er^{3+}$- and $Yb^{3+}$-sensitized strontium bismuth titanate nanoparticles, J. Alloys Compd. 801 (2019) 1–9, https://doi.org/10.1016/j.jallcom.2019.06.100.

[15] C.H. Hervoches, A. Snedden, R. Riggs, S.H. Kilcoyne, P. Manuel, P. Lightfoot, Structural behavior of the four-layer aurivillius-phase ferroelectrics $SrBi_4Ti_4O_{15}$ and $Bi_5Ti_3FeO_{15}$, J. Solid State Chem. 164 (2002) 280–291, https://doi.org/10.1006/jssc.2001.9473.

[16] B.J. Kennedy, Q. Zhou, Y.Kubota Ismunandar, K. Kato, Cation disorder and phase transitions in the four-layer ferroelectric aurivillius phases $ABi_4Ti_4O_{15}$ (A=Ca, Sr, Ba, Pb), J. Solid State Chem. 181 (2008) 1377–1386, https://doi.org/10.1016/j.jssc.2008.02.015.

[17] A. Prasad, A.S. Rao, G.V. Prakash, Up-conversion luminescence and EPR properties of $KGdF_4$:$Yb^{3+}$/$Tm^{3+}$ nanophosphors, Optik 208 (2020) 164536, https://doi.org/10.1016/j.ijleo.2020.164536.

[18] P. Rohilla, A.S. Rao, Linear and non-linear photoluminescence studies of $Ho^{3+}$/$Yb^{3+}$ co-doped titanate phosphors for photonic applications, J. Alloys Compd. 928 (2022) 167156, https://doi.org/10.1016/j.jallcom.2022.167156.

[19] F. Liu, D. Deng, M. Wu, B. Chen, L. Zhou, S. Xu, Luminescent and thermometric properties of dual emitting $Eu^{3+}$/$Sm^{3+}$ co-doped $Sr_4La(PO_4)_3O$ phosphor based on energy transfer *, J. Rare Earths 39 (2021) 261–268, https://doi.org/10.1016/j.jre.2020.06.003.

[20] Ravita A. Prasad, P. Rohilla, R. Bajaj, Anu R. Punia, A.S. Rao, Luminescence studies on $Dy^{3+}$ Doped Calcium Aluminum Borosilicate (CABS) glasses for white light emission and applications in w-LEDs, J. Fluoresc. (2023), https://doi.org/10.1007/s10895-023-03389-8.

[21] S. Kumari, A.S. Rao, R.K. Sinha, Structural and photoluminescence properties of $Sm^{3+}$ ions doped strontium yttrium tungstate phosphors for reddish-orange photonic device applications, Mater. Res. Bull. 167 (2023) 112419, https://doi.org/10.1016/j.materresbull.2023.112419.

[22] M.K. Sahu, M. Jayasimhadri, K. Jha, B. Sivaiah, A.S. Rao, D. Haranath, Synthesis and enhancement of photoluminescent properties in spherical shaped $Sm^{3+}$/$Eu^{3+}$ co-doped $NaCaPO_4$ phosphor particles for w-LEDs, J. Lumin. 202 (2018) 475–483, https://doi.org/10.1016/j.jlumin.2018.06.002.

[23] D. Jiang, L. Geng, S. Zhou, Y. Wang, Photoluminescence properties and energy transfer in the $Sm^{3+}$ and $Eu^{3+}$ co-doped $Ca_3Bi(PO_4)_3$ red phosphor, Inorg. Chem. Commun. 142 (2022) 109668.

[24] X. Min, Z. Huang, M. Fang, Y.G. Liu, C. Tang, X. Wu, Energy transfer from $Sm^{3+}$ to $Eu^{3+}$ in red-emitting phosphor $LaMgAl_{11}O_{19}$:$Sm^{3+}$, $Eu^{3+}$ for solar cells and near-ultraviolet white light-emitting diodes, Inorg. Chem. 53 (2014) 6060–6065, https://doi.org/10.1021/ic500412r.

[25] H. Thakur, R.K. Singh, A.K. Gathania, Synthesis and optical properties of $GdVO_4$: $Eu^{3+}$ phosphor, Mater. Res. Express 8 (2021) 026201.

[26] J. Huang, Q. Li, D. Chen, Preparation and luminescence properties of $Ca_3(VO_4)_2$: $Eu^{3+}$, $Sm^{3+}$ phosphor for light-emitting diodes, Mater. Sci. Eng. B 172 (2010) 108–113, https://doi.org/10.1016/j.mseb.2010.04.031.

[27] A.Y. Madkhli, H. Kaynar, M.B. Coban, M. Ayvacikli, A. Canimoglu, N. Can, Characterization, room and low temperature photoluminescence of yttrium aluminium borate activated with $Sm^{3+}$ ions, Mater. Res. Bull. 161 (2023) 112167, https://doi.org/10.1016/j.materresbull.2023.112167.

[28] G. Souadi, Ü.H. Kaynar, M. Ayvacikli, N. Can, Luminescence of undoped and $Eu^{3+}$ activated zinc gallate phosphor: synthesis, unusual intense $^5D_0 \rightarrow {}^7F_4$ red emission, Appl. Radiat. Isot. 199 (2023) 110905, https://doi.org/10.1016/j.apradiso.2023.110905.

[29] J. Zheng, X. Wu, Q. Ren, W. Bai, Y. Ren, M. Wang, O. Hai, Investigation of luminescence properties and energy transfer in $Sm^{3+}$ and $Eu^{3+}$ co-doped $Sr_3Y(BO_3)_3$ red phosphors, Opt. Laser Technol. 122 (2020) 105857, https://doi.org/10.1016/j.optlastec.2019.105857.

[30] S. Kumari, A.S. Rao, R.K. Sinha, Investigations on photoluminescence and energy transfer studies of $Sm^{3+}$ and $Eu^{3+}$ ions doped $Sr_9Y_2W_4O_{24}$ red emitting phosphors with high color purity for w-LEDs, J. Mol. Struct. 1295 (2024) 136507, https://doi.org/10.1016/j.molstruc.2023.136507.

[31] Q. Yang, G. Li, Y. Wei, H. Chai, Synthesis and photoluminescence properties of red-emitting $NaLaMgWO_6$:$Sm^{3+}$,$Eu^{3+}$ phosphors for white LED applications, J. Lumin. 199 (2018) 323–330, https://doi.org/10.1016/j.jlumin.2018.03.011.

[32] P. Rohilla, A.S. Rao, Synthesis optimization and efficiency enhancement in $Eu^{3+}$ doped barium molybdenum titanate phosphors for w-LED applications, Mater. Res. Bull. 150 (2022) 111753, https://doi.org/10.1016/j.materresbull.2022.111753.

[33] S. Kumari, A.Prasad Anu, P. Rohilla, A.S. Rao, Prospective applications of thermally stable $Dy^{3+}$ doped potassium zinc strontium borate (KZSB) glasses in w-LEDs, J. Mater. Sci. Mater. Electron. 34 (2023), https://doi.org/10.1007/s10854-023-10272-6.

[34] H. Guo, Q. Shi, K.V. Ivanovskikh, L. Wang, C. Cui, P. Huang, A high color purity red-emission phosphor based on $Sm^{3+}$ and $Eu^{3+}$ co-doped $Ba_3Bi(PO_4)_3$, Mater. Res. Bull. 126 (2020) 110836, https://doi.org/10.1016/j.materresbull.2020.110836.

[35] K. Hamraoui, M. Ferhi, M. Ferid, Color temperature tunable of $Dy^{3+}$ -doped $LaPO_4$ nanorods prepared via hydrothermal method for white LEDs applications, Opt. Mater. (Amst). 84 (2018) 852–863, https://doi.org/10.1016/j.optmat.2018.08.014.

[36] R. Bajaj, A. Prasad, A.V.S. Yeswanth, P. Rohilla, S. Kaur, A.S. Rao, Down-shifting photoluminescence studies of thermally stable $Dy^{3+}$ ions doped borosilicate glasses for optoelectronic device applications, J. Mater. Sci. Mater. Electron. 33 (2022) 1–12, https://doi.org/10.1007/s10854-021-07667-8.

[37] P. Rohilla, A.S. Rao, Energy transfer induced colour tunable photoluminescence performance of thermally stable $Sm^{3+}$/$Eu^{3+}$ co-doped $Ba_2MoTiO_6$ phosphors for white LED applications, J. Mater. Sci. Mater. Electron. 34 (2023) 1–19, https://doi.org/10.1007/s10854-023-11025-1.

[38] G. Ouertani, K. Maciejewska, W. Piotrowski, K. Horchani-Naifer, L. Marciniak, M. Ferhi, High thermal stability of warm white emitting single phase $GdPO_4$: $Dy^{3+}$/$Sm^{3+}$ phosphor for UV excited wLEDs, J. Lumin. 265 (2024) 120228, https://doi.org/10.1016/j.jlumin.2023.120228.

[39] R. Cui, X. Wang, Q. Chen, C. Deng, Photoluminescence properties and energy transfer of $ZnNb_2O_6$: $Eu^{3+}$, $Sm^{3+}$ orange-red phosphors for WLEDs, Optik 261 (2022) 169116, https://doi.org/10.1016/j.ijleo.2022.169116.